Pollutant emissions and diesel oxidation catalyst performance at low ambient temperatures in transient load conditions.

José Manuel Luján, Héctor Climent *, Luis Miguel García-Cuevas, Ausias Moratal

CMT Motores Térmicos, Universitat Politècnica de València, Spain

*Corresponding author: hcliment@mot.upv.es. Telephone: (+34) 96 387 76 50. Postal address: CMT Motores Térmicos. Universitat Politècnica de València. Camino de Vera s/n. 46022. Valencia. Spain.

Abstract

In this paper an experimental analysis of the ambient temperature effect on diesel engine pollutant emissions is carried out. The study is focused on hydrocarbons and carbon monoxide of both engine out pollutants formation analysis and diesel oxidation catalyzer (DOC) performance. The experiments were carried out at transient engine load conditions of Worldwide harmonized Light vehicles Test Cycle (WLTC) at two levels of ambient temperature: 20ºC and -7ºC. The study presented in this work shows significant different results depending on the pollutant analysed. Regarding hydrocarbons, a significant dependence of pollutant formation on ambient temperature is observed, being the emissions at -7 ºC between two and three times the emissions at 20 ºC. The DOC performance between temperatures shows similar conversion efficiency. In the case of carbon monoxide formation, temperature dependence plays a less important role than the engine load conditions. The reduction of air fuel ratio at transient conditions drives to unsteady CO profiles emissions along the WLTC that reduce the pollutant conversion with a greater negative impact at -7 ºC.

Keywords

Diesel oxidation catalyzer; Engine out emissions; Cold conditions; Transient engine loads.

1. Introduction

Pollutant emissions in automotive diesel engines have become as a major subject of research. Hydrocarbons (HC), carbon monoxide (CO), nitrogen oxides (NOx) and particles are the main pollutants emitted in combustion diesel engines [1, 2, 3, 4, 5 , 6 and 7]. Catalytic converters have been used in engine exhaust after treatment systems for more than two decades to reduce pollutant emissions [8]. Diesel oxidation catalysts (DOC) are used to control CO, HC and the organic fraction of diesel particulates to form harmless exhaust products. Additional reactions such as the oxidation of NO to NO_2 also occurs with the key interest attributed in facilitating passive diesel particulate filter (DPF) regenerations as well as in enhancing the performance of some selective catalytic reductions (SCR) catalysts [9].

Salomons et al. [10] studied the effect of CO and H_2 concentration on the catalysis performance, showing the increase of light off temperature with the CO concentration and the decrease of light off with the H_2 concentration. In addition to the pollutants concentrations effect, Zervas [11] analysed the impact of space velocity, average value and profile of exhaust temperature, on Diesel engine tail-pipe emissions, pointing out the reduction of catalysis efficiency with the space velocity because of the lower dwell time as well as the increase of conversion efficiency with higher, both average and instantaneous, exhaust temperatures. Botsaris and Sparis [12] analysed the impact of the ambient temperature on the catalyst performance, by means of catalyzer inlet-outlet temperature measurements, reporting an increase of efficiency with the ambient temperature. Karl Arnby et al. [13], studied the improvement of catalysis activity of CO performing at low temperatures by means of non-homogeneous supported catalyst.

As automotive driving cycles are being more restrictive, it is expected that the operation conditions of the test drive will consider the effect of running at lower ambient temperature. Under these conditions, pollutant emissions during the engine warm-up are critical. According to the literature [14] and [15], unburned hydrocarbons and carbon monoxide are mainly emitted when engine temperatures remain low. Researchers have study the effect on pollutant emissions and engine performance in cold driving cycles [16, 17, 18 and 19]. Currently, the U.S Environmental Protection Agency includes a cold cycle of FTP-75 as an optional driving cycle

carried out at -7 ºC. It is expected that if future regulations include cold cycles as mandatory, they will be assessed at this temperature.

In this work, the effect of cold ambient temperature on the engine-out emissions as well as on the pollutants conversion efficiency at the DOC is analysed. The pollutants studied are hydrocarbons and carbon monoxide. The tests were carried out at transient engine load conditions of WLTC at -7 ºC and 20 ºC of ambient temperature.

The paper is structured as follows. Section 2 is devoted to the experimental setup and the explanation of the theoretical models and tools. Section 3 contains the results and analysis of the ambient temperature effect on the engine-out emissions and on the DOC performance. Finally, the main conclusions are presented in section 4.

2. Experimental setup and methodology

2.1. Description of test cell and setup.

Experiments with an inline 4 cylinder, 1.6 l, turbocharged HSDI diesel engine were conducted. In Fig. 1 the engine layout is depicted, where both the High Pressure (HP) and Low Pressure (LP) Exhaust Gas Recirculation (EGR) loops are shown. An intercooler is placed between the compressor and the HP EGR inlet. The aftertreatment system formed by the DOC and DPF is placed downstream the turbine.

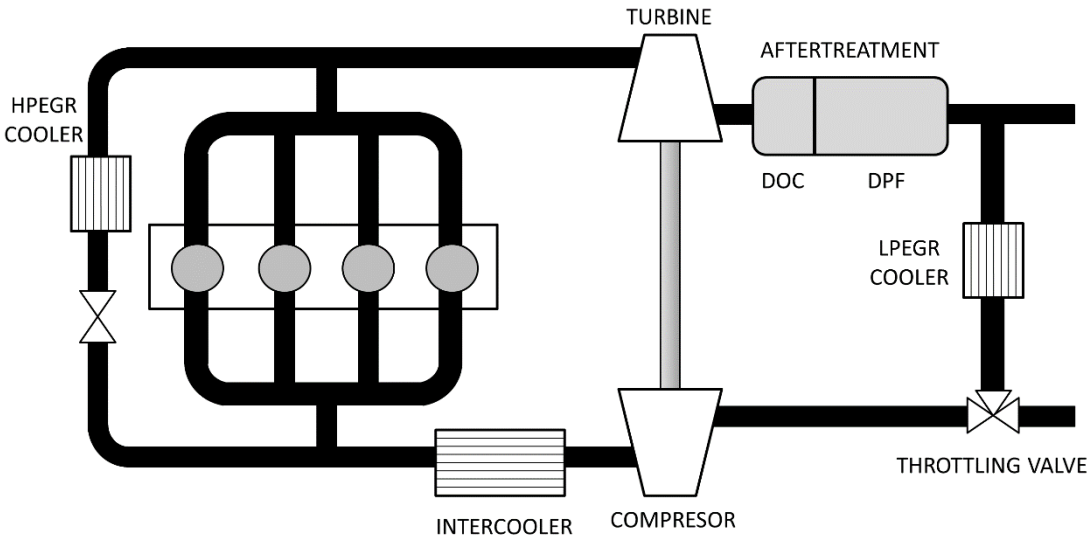

Fig 1. Engine layout.

The tests were carried out in a climatic chamber where the ambient, coolant and fuel temperatures are under control. In Table 1 the features of the engine are shown. The engine

was run under transient state conditions of a WLTC driving cycle. Once the WLTC has finished, the engine is put under specific conditions of load to regenerate the particulate filter. After that, test cell is cooled for several hours in order to ensure the same initial conditions of all cycles carried out.

Table 1.

Engine specifications.

Cylinder number	In-line 4
Bore x stroke (mm)	80 x 79.5
Displacement (cm3)	1598
Compression ratio	15.4:1
Valve number	16
Valvetrain	Double cam shaft over head
Fuel delivery system	Common rail. Direct injection.
EGR system	HP and LP cooled EGR
Intake boosting	Turbocharger with VGT
Maximum power (kW/rpm)	96/4000
Maximum torque (Nm/rpm)	320/1750
Torque at maximum power (Nm)	315
Specific power (kW/liter)	60.86

Relevant variables of the test needed for the analysis were recorded: engine speed, torque, intake manifold pressure, turbine inlet pressure, intake manifold temperature, air mass flow rate, fuel consumption and chemical species such as carbon monoxide (CO), hydrocarbons (HC), oxygen (O_2) and carbon dioxide (CO_2). All measurement signals were sampled at 10 Hz.

Engine speed was measured through a KYSTLER encoder with an uncertainty of 0.02 Crank Angle Degree (CAD). Engine torque was measured by the SCHENK DYNAS3 dynamometer, with an error of 0.1%. The engine speed and torque are the engine target variables needed to perform the WLTC. Both variables are calculated from the vehicle velocity and the gear ratio defined by the WLTC and the characteristics of the vehicle. The vehicle model used for the tests was a typical mid-size car from the European market. The calculation process of the driving cycle target variables is as follows:

The engine speed is calculated from the vehicle speed and gear according to the following expression:

$$n = \frac{u}{\pi \cdot D \cdot Z} \quad [1]$$

Where n is the engine speed, Z is the gearbox ratio between the driven and the drive gear, u is the vehicle speed and D is the diameter of the car wheel.

The engine power demand is calculated from the increase of vehicle kinetic power, the loss terms and the mechanical efficiency of the gearbox.

$$P = \left(\frac{\frac{m}{2} \cdot (u^2{}_{t+1} - u^2{}_t)}{t} + P_{road} + P_{air} \right) \cdot \frac{1}{\eta_m} \quad [2]$$

Where P is the crankshaft power, m is the vehicle mass, u is the vehicle speed, t is the time between two points of the WLTC, P_{road} is the road friction power loss, P_{air} is the aerodynamic power loss and η_m is the mechanical efficiency of the gear box. The first term of the sum represents the increase of kinetic power of the vehicle. In case of no velocity variation, the demand of power is only because of the frictional losses. Road and aerodynamic friction losses are vehicle speed depending.

Once the crankshaft power and the engine speed are obtained the engine torque, T, is calculated as:

$$T = \frac{P}{n} \quad [3]$$

Temperatures were measured with type K thermocouples of TCA brand, with a measurement error of 2.2 K. Gas pressure was measured with KISTLER pressure sensors with an error of 0.3%. Air mass flow rate was measured by means of a hot wire anemometer of Sensyflow brand, with a measurement error of 0.1%. Fuel consumption along the WLTC cycle was measured with an AVL fuel balance, with a measurement error of 0.12%.

A HORIBA MEXA ONE gas analyser was used to measure the exhaust gas chemical composition at both upstream and downstream DOC sample points. O_2 was measured by means of a magnetopneumatic detector. CO was measured by using non-dispersive infrared techniques. HC was measured by means of the the flame ionization detection technique. In case of CO_2 it was measured at the intake manifold as an additional sample point for Exhaust Gas Recirculation (EGR) rate calculation, by means of non-dispersive infrared techniques. The uncertainty of the gas analyser is in the range of 2%.

Both intake and exhaust, upstream DOC, CO_2 measurements were recorded in order to obtain the LP EGR rates. The EGR rate is defined as:

$$X_{\mathrm{EGR}} = \frac{\dot{m}_{\mathrm{egr}}}{\dot{m}_{\mathrm{air}} + \dot{m}_{\mathrm{egr}}} \quad [4]$$

Where $\dot{m}_{\mathrm{egr}}$ and $\dot{m}_{\mathrm{air}}$ are the mass flow of EGR gas and fresh air, respectively. Eq. 4 can be expressed as a function of a specific pollutant molar concentration, like CO_2, measured in the intake and exhaust manifold:

$$X_{EGR} = \frac{[CO_{2\,\mathrm{INT}}] - [CO_{2\,\mathrm{ATM}}]}{[CO_{2\,\mathrm{EXH}}] - [CO_{2\,\mathrm{ATM}}]} \quad [5]$$

Where $[CO_{2\,\mathrm{INT}}]$, $[CO_{2\,\mathrm{ATM}}]$ and $[CO_{2\,\mathrm{EXH}}]$ are the carbon dioxide concentration in the intake, ambient and exhaust place respectively.

2.2. Pollutant emissions calculation

Once the chemical pollutants have been measured by the gas analyser, it is necessary to process the data to ensure the right time span and avoid the mismatch between pollutant emissions and the other engine variables such as air and fuel mass flow [20]. The existence of a delay in pollutant analysis is due to two different sources [21]. On one hand, there is an internal delay necessary to analyse the sample that depends on the type of pollutant. On the other hand the distance between the sample point and the gas analyser forces the existence of a delay defined by the gas velocity and the length of the sample pipes. The gas speed through the sample pipes is produced by the vacuum pressure generated by the gas analyser pump, which remains equal during the whole cycle. Some authors have implemented physical behavior models [22] while other authors analyse the delay by correlation methods comparing the pollutant measurement with other related variables like engine speed and air mass flow rate [23]. In this study a correlation method is used, based on the convolution between pollutants and air mass flow signals [24]. Convolution expresses the amount of overlap between two functions; it is defined as the integral of the product of two signals when one of these functions is shifted over the other:

$$(p * m)(t) = \int_{-\infty}^{+\infty} p(t) \cdot m(t - \varphi) d\tau \cong \sum_{i=0}^{i=n} p_i \cdot m_{i-k} \quad [6]$$

Where p and m are the pollutant and air mass flow signals in the timed domain *(t).* φ is the shift variable. The right hand side of the equation is an approximation of the convolution between functions in case they are finite discrete signals. p_i and m_{i-k} are expressed in vector notation, where i is any point of the signal of the n measured points, k works as shift coefficient. The point where the convolution function is maximum indicates the mismatch delay between signals that have to be corrected to match both measurements.

The chemical sample point is located at both upstream and downstream the DOC to analyse the effect of the catalyser on the pollutant emissions. Flow rate mass emissions are calculated using the pollutant concentrations and the air and fuel mass flow rate, according to the equation below, in order to know how much pollutants are released to the atmosphere.

$$\dot{m}_{pollutant} = \frac{M_{pollutant}}{M_{air}} \cdot \left(\dot{m}_{air} + \dot{m}_{fuel}\right) \cdot \left[C_{pollutant}\right]^{*} \qquad [7]$$

Where $M_{\mathrm{pollutant}}$ and M_{air} are the molecular weight of pollutants and air respectively $\dot{m}_{\mathrm{air}}$ and $\dot{m}_{\mathrm{fuel}}$ are the mass flow of fresh air and fuel respectively and $\left[C_{\mathrm{pollutant}}\right]^{*}$ is the corrected pollutant concentration. Species concentration measurements such as CO, CO_2 and NO_x are carried out in dry basis, so the concentration is corrected in order to take into account the exhaust gas water vapor content because of the combustion as well as the ambient humidity where the chemical products are being released. Pollutant measurements are corrected according to European Commission Directive 2001/63/EC of 17 August 2001 adapting to technical progress Directive 97/68/EC [25].

2.3 Repeatability and test uncertainty calculation

In addition to the errors of the measurement devices, engine performance and boundary test conditions variability affects the result obtained. Beyond the accuracy of the engine actuators and sensors such as fuel injectors, variable geometry turbine position control and engine speed encoder between others, it is observed a variability when the same test is performed several times. In order to quantify the natural variability of the process and define which tests are under control and which can be considered as outliers, a procedure for anomalous results detection is defined. The outlier detection methodology is divided in two parts. The first part calculates the weighted average of the relative error of test variables. The relative error is weighted by means

of the instantaneous variable measurement magnitude. The mathematical expression is shown below, where the right hand side is the discrete approximation according to Riemann Sum.

$$\varepsilon = \frac{\int_0^T \bar{\beta}(t)\cdot\bar{x}(t)\,dt}{\int_0^T \bar{x}(t)\,dt} \cong \frac{\sum_{i=0}^{i=n} \bar{\beta}_i\cdot\bar{x}_i}{\sum_{i=0}^{i=n} \bar{x}_i} \quad [8]$$

Where $\bar{x}$ is the instantaneous measured average variable, $\bar{\beta}$ is the instantaneous average relative error of each variable, both obtained from the mean of several repetitions of the same test, and n is the number of test measurement points. $\bar{\beta}$ is calculated as follows:

$$\bar{\beta} = \frac{1}{m}\cdot\sum_{j=0}^{j=m}\alpha_j \quad [9]$$

Where m is the number of test repetitions by case and α is the instantaneous relative error of each test repetition defined as:

$$\alpha_j = \frac{x_j-\bar{x}}{\bar{x}} \quad [10]$$

Where x is the variable under study at the j test repetition. Measured variables, such as pressures, temperatures, fuel mass flow, air mass flow, engine speed, engine torque show a relative error (ε) lower than 5%.

The second part of the outlier detection method focusses on pollutant emissions variability. Because pollutants emissions variation between test repetitions can be high compared to the rest of the test variables [21], an additional analysis based on cumulative emissions instead of instantaneous measurements is applied. The pollutant mass is calculated at the key points of the WLTC test: low load, middle load, high load and extra high load. The pollutants dispersion degree is analysed by means of boxplots where data is divided in quartiles. The threshold to consider a measurement as an outlier is when the distance between the pollutant mass and the closest quartile is higher than 1.5 times the interquartile range. In addition, extreme values existence is studied though the comparison of the mean and median of the data set. In case of adding an anomalous test in a sample, the median remains with low variations while the mean is strongly modified. The comparison between median and mean is characterised by the ratio between the absolute difference between the median and mean divided by the median of the data set:

$$SK = \frac{|m-\mu|}{m}\cdot 100\ (\%) \quad [11]$$

Where SK is the median-mean skewness coefficient, m and μ are the pollutant median and average of the test, respectively, at each defined time step. This coefficient measures the central tendency of the data set distribution. Taking into account that the experimental uncertainty variability as a symmetric distribution, the higher this coefficient is the skewed the data set because of the presence of an outlier. The threshold of this coefficient, to consider a measurement as an outlier, is defined as 4%. The threshold value is obtained by statistical simulation approach: first, considering the hypothesis of normal error pollutants distribution [26] it is created a normal distribution with a mean and a standard deviation obtained from the experimental data set. Then, a large data set is randomly sampled and used to calculate the average of the median-mean skewness coefficient. This procedure is applied at each key point of the driving cycle by pollutant emission. Finally, the highest value obtained of the averaged skewness coefficients is defined as threshold of the SK coefficient.

2.4 Experimental data analysis tools

Pollutant emissions are analysed at the inlet and outlet of the DOC at both low (-7 ºC) and high (20 ºC) ambient temperatures. Effect of ambient temperature on pollutants formation is analysed by means of engine-out emissions through the DOC inlet measurement comparison between cases performed at different ambient temperatures. DOC performance analysis is carried out for CO and HC emissions. The catalyser efficiency is defined as follows:

$$\eta = \frac{[X_i]-[X_o]}{[X_i]} \qquad [12]$$

Where $[X_i]$ and $[X_o]$ are the pollutant concentration at the inlet and outlet of the DOC respectively.

According to several authors [8] and [11], DOC temperature, dwell time, [O_2], [CO] and [HC] are the test variables that play a key role in the DOC performance. Dwell time is calculated as:

$$\tau = \frac{V_{DOC} \cdot \rho}{\dot{m}_{exh}} \qquad [13]$$

Where $\dot{m}_{exh}$ is the exhaust mass flow, V_{DOC} is the internal DOC volume and ρ is the gas density calculated from the ideal gas law:

$$\rho = \frac{p}{R \cdot T} \qquad [14]$$

Where p is the exhaust pressure, R the ideal gas constant and T the gas temperature.

2.5 Catalysis temperature estimation

DOC inner temperature plays an important role for DOC performance analysis. However, DOC inner measurements are difficult to achieve because of technical restrictions. Firstly, the small honeycomb channel section would be partially blocked by the presence of a thermocouple, disturbing the gas flow through the channel. Secondly, the small space available for temperature sensing makes it difficult to ensure the right position of the sensor during the tests realization. Finally, to perform the honeycomb bulk temperature measurement it would be needed to drill the DOC housing with the risk of damaging the ceramic honeycomb. Taking into account the aforementioned drawbacks, a DOC temperature estimation model is proposed.

The temperature estimation is based on a nodal heat transfer model where the thermal inertia, surrounding heat losses and internal heat generation are considered. The estimated temperature, named in this paper as DOC reference temperature, represents an average temperature of the whole DOC. The variables needed for the model implementation are: the exhaust gas temperatures and chemical species concentration at the inlet and outlet of the DOC, the exhaust mass flow and the surrounding air room temperature where the DOC is placed. The DOC reference temperature is averaged with the mean DOC internal exhaust gas temperature in order to obtain the estimated catalysis temperature. This temperature represents the mean temperature of the solid-gas interface where catalysis takes place. The catalysis temperature estimation is defined as follows:

$$T_{\text{catalysis}} = \frac{T_{\text{DOC}} + T_{\text{gas\_mean}}}{2} \quad [15]$$

Where T_{DOC} is the DOC reference temperature and $T_{\text{gas\_mean}}$ is the mean gas temperature of the inlet and outlet of the DOC.

Regarding the model for DOC reference temperature calculation, the DOC is formed by a ceramic honeycomb and a steel housing. Due to the small thickness of the steel housing, both parts are merged in the model and considered as one bulk. The heat released in the DOC comes from the exhaust gas enthalpy and the reaction enthalpy of the chemicals species oxidation. The heat losses to the surroundings are calculated considering natural convection heat transfer. The DOC reference temperature evolution over time is calculated according to the following expression:

$$T_{\mathrm{DOC}}{}^{t+1} = \left(\dot{\mathrm{H}}^{\mathrm{t}} - \left(T_{\mathrm{DOC}}{}^{t} - T_{\mathrm{amb}}{}^{t}\right) \cdot h_{\mathrm{ext}}{}^{t} \cdot A_{\mathrm{ext}}\right) \cdot \frac{\tau^{t}}{\rho_h \cdot V_h \cdot C_h + \rho_s \cdot V_s \cdot C_s} \quad [16]$$

Where $\dot{\mathrm{H}}$ is the internal generation of thermal power released in the DOC, T_{amb} is the ambient temperature in the test cell, h_{ext} is the convective heat transfer coefficient, A_{ext} is the exterior surface of the DOC housing, $\rho_h \cdot V_h \cdot C_h$ and $\rho_s \cdot V_s \cdot C_s$ are the density, volume and specific heat of the honeycomb and the steel DOC housing respectively. The superscript indicates the time instant along the WLTC.

The convective coefficient of the natural convection is calculated according to Morgan's correlations [27] of the Nusselt number by means of the Grashof and Prandtl number calculation.

The DOC internal generation has two energy terms. On one hand, the heat coming from the exhaust gases, calculated as:

$$\dot{H}_{exh} = \dot{m}_{\mathrm{exh}} \cdot c_{\mathrm{exh}} \cdot \left(T_{\mathrm{DOC\_i}} - T_{\mathrm{DOC\_o}}\right) \quad [17]$$

Where $\dot{m}_{\mathrm{exh}}$ is the exhaust mass flow passing through the DOC, c_{exh} is the exhaust gases specific heat, $T_{\mathrm{DOC\_i}}$ and $T_{\mathrm{DOC\_o}}$ are the inlet and outlet DOC gas temperatures.

The other term of the internal generation concerns the enthalpy released by the oxidation of carbon monoxide and hydrocarbon species. The proposed reaction mechanism is based on a set of one elementary step reactions. CO mechanism is shown below:

$$CO + \frac{1}{2} \cdot O_2 \rightarrow CO_2 \quad [18]$$

The specific reaction enthalpy is calculated from the balance of standard formation enthalpy of products and reactants:

$$\Delta H_r = H_f(CO_2) - H_f(CO) \quad [19]$$

Where ΔH_r is the specific reaction enthalpy and H_f is the formation enthalpy of the correspondent compound.

In the case of hydrocarbons measurement, the FID technique (Section 2.1) doesn't allow to know the concentration of each hydrocarbon species. The HC measurement is obtained as an equivalent methane molar concentration. According to the bibliography, diesel engines hydrocarbon emissions are mainly formed by light alkenes along with medium-heavy alkanes

[28] and [29]. The general reaction formulation for alkanes and alkenes (only monounsaturated considered) used is:

$$C_xH_{2\cdot x+2} + \left(\frac{3\cdot x+1}{2}\right)\cdot O_2 \rightarrow x\cdot CO_2 + (x+1)\cdot H_2O \quad \text{Alkanes} \qquad [20]$$

$$C_xH_{2\cdot x} + \left(\frac{3}{2}\cdot x\right)\cdot O_2 \rightarrow x\cdot CO_2 + x\cdot H_2O \quad \text{Alkenes} \qquad [21]$$

The HC concentration measurement and the standard enthalpy of formation are weighted according to the hydrocarbons species distribution study by Stanislav V. Bohac et al. [30] for a conventional diesel combustion engine running at 1500 rpm and 3.9 bar of break mean effective pressure (BMEP), that are representative conditions of the engine speed and BMEP average values of the performed WLTC tests. The set of reactions include fifteen hydrocarbons, parafine and oleofine species, from methane to pentadecane. The enthalpy of formation of the products is corrected as follows:

$$H_f(X_i)\_\text{corr} = H_f(X_i)\cdot\sum_{i=1}^{i=15} c_i\cdot A_i \qquad [22]$$

Where $H_f(X_i)$ is standard enthalpy of formation without correction for CO_2 or H_2O,

c_i is the concentration of each species referred to the total amount of hydrocarbons and $\mathrm{A_i}$ is the products stoichiometric index according to the formulation shown at Eq. 20 and Eq. 21.

In the case of reactants, the correction includes the standard enthalpy of formation of each hydrocarbon species as:

$$H_f(HC)\_\text{corr} = \sum_{i=1}^{i=15} c_i\cdot H_f\left(C_xH_y\right)_i \qquad [23]$$

Where $H_f\left(C_xH_y\right)_i$ is the standard enthalpy of formation of each hydrocarbon species. The stoichiometric index is not included because it is defined as one according to the formulation shown previously in Eq. 20 and Eq. 21.

In addition to the enthalpy of formation, the hydrocarbon concentration measured by the FID has to be corrected too. The hydrocarbons concentration is corrected taking into account the number of carbon atoms of each species according to the following expression:

$$f = \frac{1}{\sum_{i=1}^{i=15} c_i\cdot n_i} \qquad [24]$$

Where f is the concentration factor to be applied to the HC concentration measurement and n_i is the number of carbon atoms by hydrocarbon species.

Once both the enthalpy of formation correction and the concentration factor are calculated, the corrected specific reaction enthalpy is obtained as:

$$\Delta H_{\mathrm{r\_corr}} = f \cdot \left(H_f(CO_2)_{\mathrm{corr}} + H_f(H_2O)_{\mathrm{corr}} - H_f(HC)_{\mathrm{corr}}\right) \quad [25]$$

3. Results and discussion

This section is divided in two parts. First the effect of the ambient temperature on the combustion process is analysed trough the engine out pollutants measurement. Secondly, the DOC performance variation because of the ambient temperature is covered by means of conversion efficiency comparison.

3.1 Effect of ambient temperature on engine performance and pollutants formation.

WLTC cycles are performed at two ambient temperatures: -7ºC and 20ºC. Fig.2 depicts the temperature measured in the intake manifold downstream the intercooler before the HP-EGR mixer at both ambient temperatures. The top intake temperature (dotted red line) belongs to the 20 ºC case while the lowest intake temperature (solid blue line) belongs to the case at -7 ºC. The gray area represents the vehicle speed during the WLTC cycle. A similar temperature evolution is shown in both cycles: as the engine load increases along the cycle the intake temperature increases.

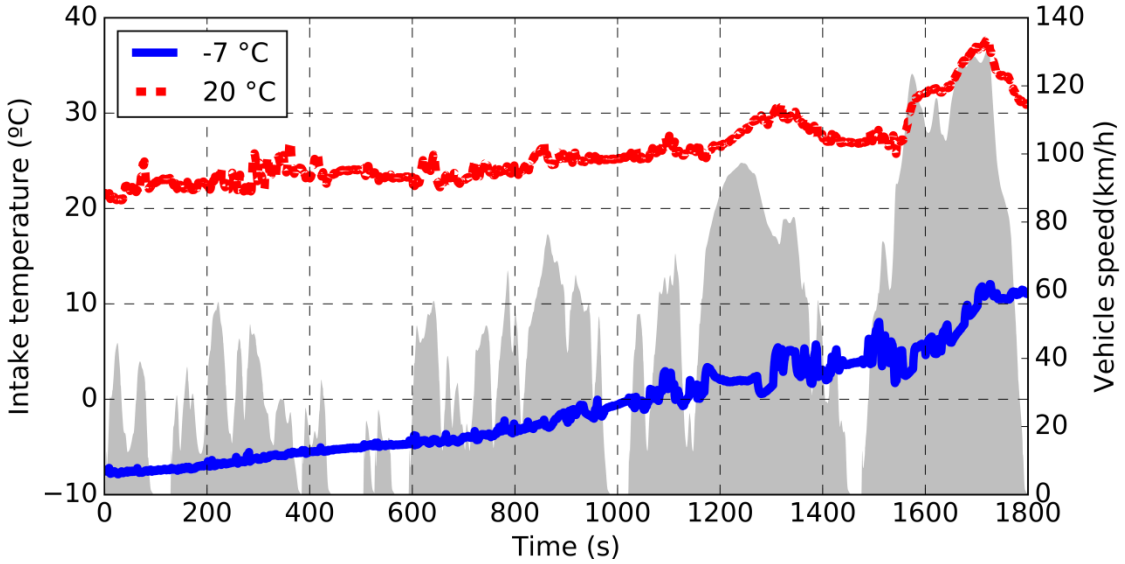

Fig 2. Intake temperatures of WLTC cycles at different ambient temperatures, -7 ºC in solid blue line and 20 ºC in dotted red line. The gray area shows the vehicle speed at the WLTC cycle.

In Fig. 3 the coolant and oil temperatures are shown for both ambient temperatures. On one hand, coolant and oil temperatures evolve in similar manner by case. On the other hand, comparing between the different ambient temperatures, the initial temperature difference of 27 ºC roughly remains along the WLTC, pointing that the warmup evolves in both cases in a similar way. The higher heat transfer to the surroundings and mass heating in the case of – 7ºC doesn't affect the coolant and oil heating rate because the amount of injected fuel is higher at -7 ºC than at 20 ºC. According to the figure 4 the fuel consumption is up to 30% higher in the case of -7 ºC at the beginning of the WLTC cycle. Once the coolant and oil temperatures reach 80 ºC, the radiator cooling system is enabled by means of the thermostat opening. After 1300 seconds, when high and extra high loads are performed, both cases -7 ºC and 20 ºC show the same coolant and oil temperatures. As the warm up proceeds the temperature of both fluid increases and the fuel consumption ratio between cases decreases. When the high loads are performed, temperatures are at the same level and fuel ratio is close to one.

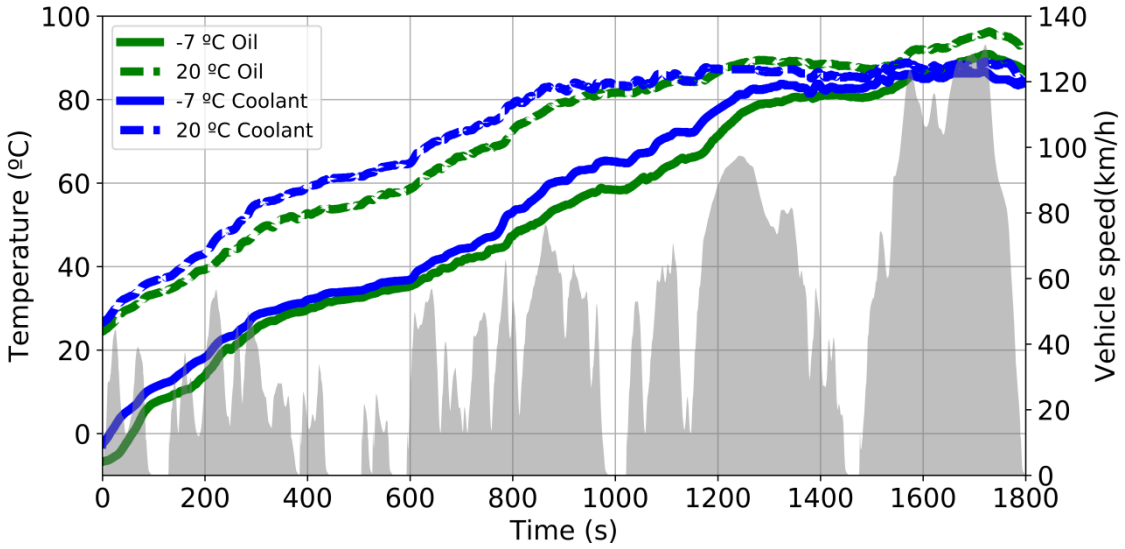

Figure 3. Engine coolant (blue lines) and oil temperatures (green lines) temperature evolution along the WLTC cycle at -7 ºC (solid lines) and 20 ºC (dotted lines). The gray area shows the vehicle speed at the WLTC cycle

The ambient temperature difference carries a significant variation of the operative engine variables, such as the intake mass flow and fuel consumption. The ratio of cumulated air mass flow and fuel consumption between the -7 ºC and the 20 ºC cases

is shown in Fig. 4. Because of the intense transient load conditions of WLTC cycles, the variables shown were averaged over the time. Both air and fuel ratio show similar profiles: at the beginning, significant reductions are observed at times from 100 to 300 s, due to the engine warming up. Then, due to the reduction on engine load at the last part of the low load part of the WLTC, a flat evolution is observed in fuel ratio and an increase of air mass ratio is noticed. From the 600 and 875 seconds, for fuel and air mass flow ratios respectively, the reduction of both ratios happens because of the performance of the medium, high and extra high load parts of the WLTC cycle along with the activation of HP and LP EGR at 20ºC and -7 ºC respectively. The fact that the fuel consumption is the same at the end of both WLTC cases, points out the low effect of the ambient temperature on engine efficiency when high loads are performed. The high engine loads at the WLTC speed up the warming up leading to reductions in the impact of ambient temperatures on the combustion process.

Regarding the air mass flow ratio, notable differences are observed between the two ambient temperature cases. The reason of the air mass flow difference is twofold: on one hand, the lower ambient temperature carries a higher intake air density. On the other hand, the tests are performed according to the serial engine driving calibration. So, the HP and LP EGR systems perform in different manner. The HP EGR system is enabled from the beginning of the cycle at 20 ºC, while at low ambient temperatures is not activated until the 875 seconds. Owing to the aforementioned, the cylinder trapped air mass is higher at – 7 ºC than at 20 ºC.

Regarding fuel ratio, it is observed higher fuel consumption from the beginning of the WLTC at -7 ºC. According to several authors [31] and [16] fuel consumption increases at low temperature conditions because of the heat engine losses, engine mass heating and frictional losses which are higher at low temperatures.

As the cycle proceeds, both air and fuel ratios decrease. Concerning the air mass flow, from 875 seconds the ratio begins to decrease because of the HP EGR enabling in the

-7 ºC case. In the case of fuel consumption, as the engine mass heating evolves with the WLTC, both the thermal inertia losses as well as oil frictional losses are reduced, and, therefore the fuel consumption ratio becomes lower. Finally, at the end of the WLTC, the fuel ratio between both ambient temperature nearly achieves unity.

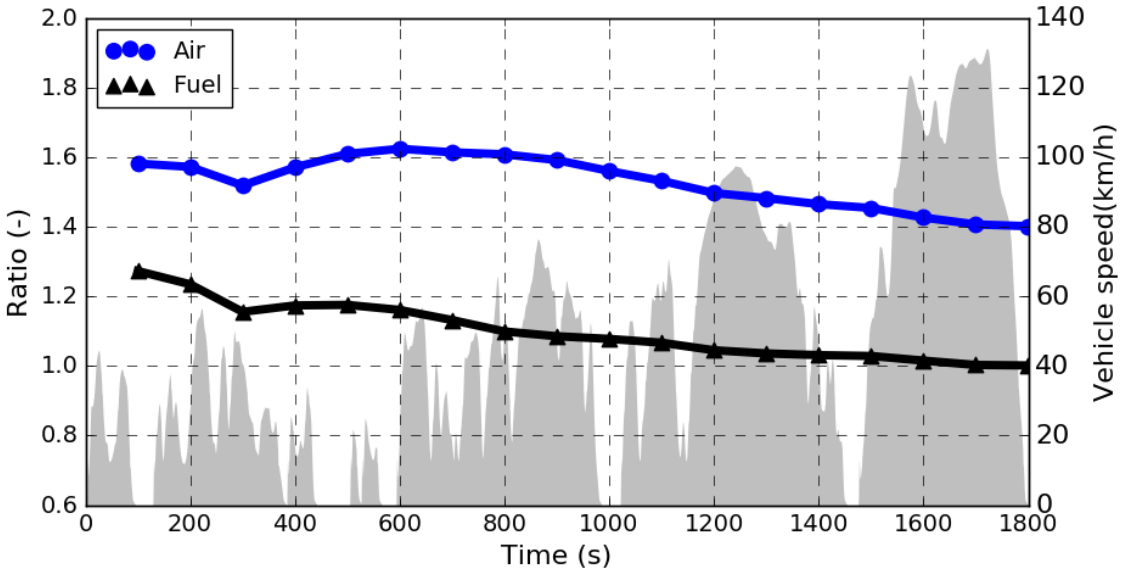

Fig. 4. Ratio of cumulative air and fuel between -7 ºC and 20 ºC cases. Air mass ratio in blue circle, fuel mass ratio in black triangles, WLTC vehicle speed is depicted as a surface in gray.

Regarding the effect of ambient temperature on pollutants formation (DOC upstream), cumulative HC and CO mass ratios between -7 ºC and 20 ºC are shown in Fig. 5. High pollutants are produced at -7ºC at the beginning of the cycle for the two species. At 200 seconds, where the last part of low load is performed, both pollutant ratios begin to reduce. The evolution of these ratios performs in different ways. While HC emissions show a quite constant reduction rate profile with the increase of the engine load along the cycle, the CO emissions are drastically reduced between 200 and 300 seconds of the WLTC. Following, at the low loads and idle condition between 300 to 600 s, it is observed a plateau behavior in CO. Once the medium load performs, the reduction carries on and finally the measured CO values at -7ºC become lower than 20 ºC with around a 20% of reduction. This fact proves the existence of additional factors beyond the ambient temperature on CO pollutants formation. While HC emissions are driven mainly by temperature, CO emissions are produced mostly because of air fuel ratio conditions. Due to the notable transient load conditions of the WLTC, uncomplete combustion can occur and therefore carbon monoxide is released as a combustion product. So, CO

formation is because of two factors: ambient temperature and air fuel ratio which plays a major role on CO release because of the high speed transient events of WLTC. The lower CO formation at -7ºC is due to the higher amount of air mass (Fig. 4) that implies higher air fuel ratio during transient conditions.

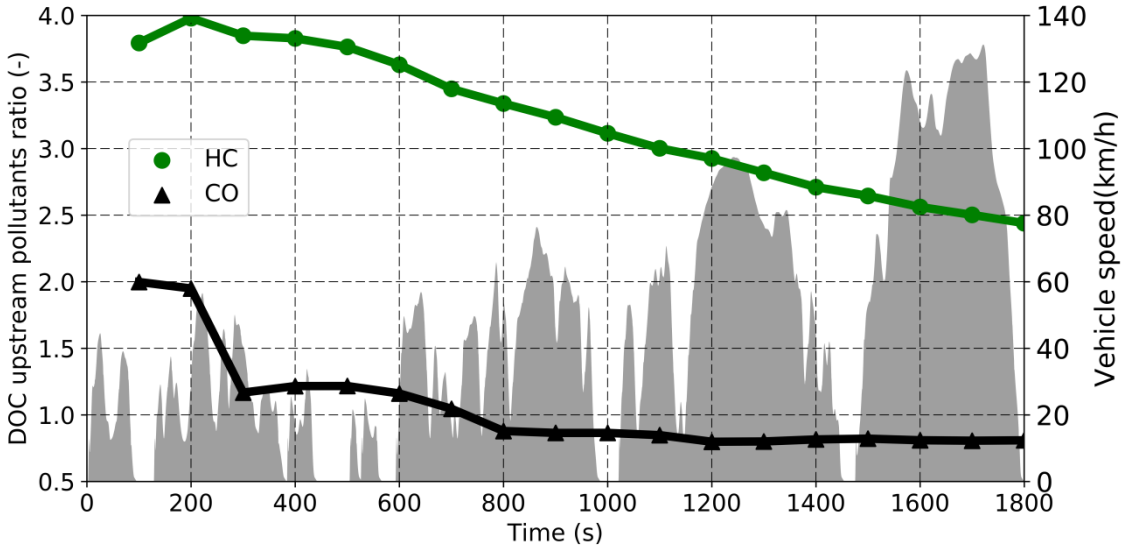

Fig. 5. Ratio of engine out (DOC upstream) cumulative THC and CO between -7ºC and 20ºC cases. THC in green circles, CO in black triangles, WLTC vehicle speed is depicted as a surface in gray.

3.2 Diesel Oxidation Catalyst performance

According to the general expression of the chemical reaction rate, along with the Arrhenius constant rate expression, the efficiency of a chemical reaction depends on the DOC temperature, dwell time and oxygen concentration at the inlet of the DOC. The conversion efficiency equation can be obtained from the general reaction rate expression, considering a single-step reaction, as follows:

$$\frac{d[X]}{dt} = [O_2]^a \cdot [X] \cdot K(T) \quad [26]$$

$$\frac{d[X]}{dt} \cong \frac{[X_i]-[X_o]}{\tau} = [O_2]^a \cdot [X_i] \cdot K(T) \quad [27]$$

The above expression is substituted in the conversion efficiency equation, Eq. 12, as:

$$\eta = [O_2]^a \cdot K(T) \cdot \tau \quad [28]$$

Where $[O_2]^a$ is the oxygen concentration raised to the a power, a is the stoichiometric coefficient of oxygen, τ is the dwell time of the gas in the DOC, $K(T)$ is the reaction rate constant, $[X_i]$ and $[X_o]$ are the DOC inlet and outlet pollutant concentration respectively.

Despite Eq. 28 doesn't take into account the pollutant concentration on DOC efficiency, several authors have reported the influence of pollutant concentration on catalyst performance. According to [10] and [32], the light-off temperature increases with the pollutant concentration. In addition, pollutants interfere between them in the catalyst process [33], encouraging the conversion rate of CO_2, in case of high monoxide concentration, due to the higher reactivity of CO respect to some hydrocarbon species.

Because of the catalysis temperatures show very similar values comparing different ambient temperatures, they are not included in the analysis for DOC efficiency differences. The estimated catalysis temperature, as detailed in section 2.5, is shown in Fig. 6. The catalysis temperatures show similar values from the beginning of the cycle. Higher temperatures are estimated at 20ºC after 800 seconds of the WLTC. The cause of such difference is twofold. On one hand the exhaust gas temperature is slightly higher at 20 ºC than at -7ºC, with an average difference of 17 ºC along the WLTC cycle. On the other hand, after the 600 seconds the HP EGR is changed to LP EGR in the case of 20 ºC case, and therefore the exhaust mass flow increases. Both higher exhaust temperature and exhaust mass flow increase drive to a higher release of thermal power in the DOC at 20 ºC when high engine loads are performed from the 800 seconds of the WLTC. The reasons why catalyst temperatures show so similar values no matter the ambient temperature are: the similar DOC inlet gas temperatures, the higher exhaust gas flow at -7ºC than 20ºC, the relative low heating losses at the DOC driven by free convection and the low thermal inertia of the DOC because of its low mass.

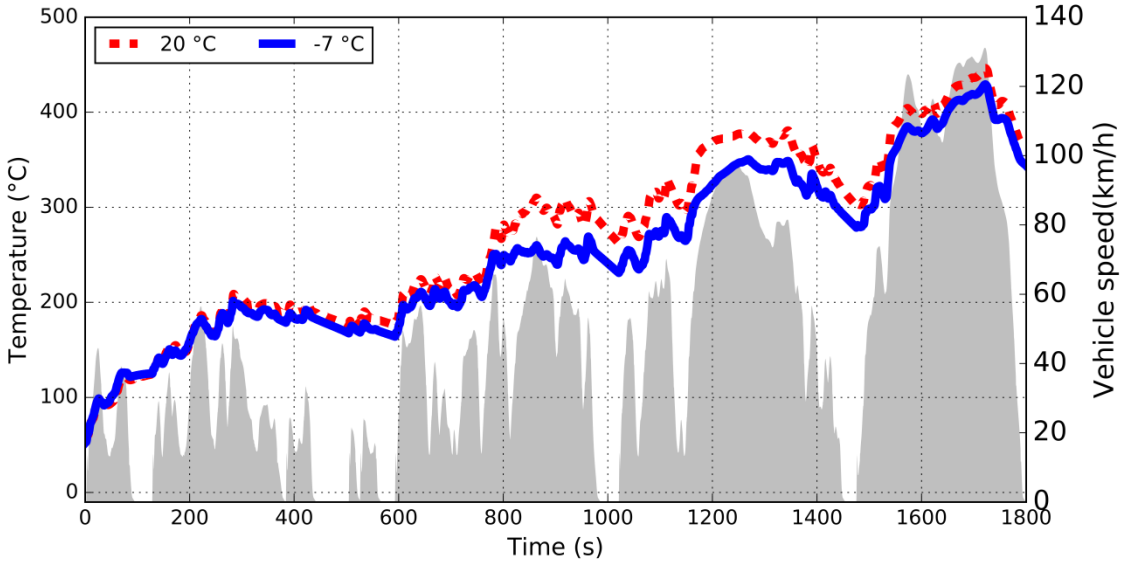

Fig. 6. Catalysis temperature evolution for -7 ºC and 20 ºC ambient temperature. WLTC vehicle speed is depicted as a surface in gray.

DOC conversion efficiencies over the WLTC are depicted in Fig. 7 for THC and CO. DOC performs with relative high efficiency from the beginning of the cycle, mainly in the case of HC conversion (70%). The high efficiency in the first instants can be explained by the adsorption of some chemical species in the washcoat that retains pollutants in the DOC. Several authors have study the adsorption and desorption mechanisms on oxidation catalyzers, [35] and [36]. The adsorption effect on pollutants conversion is beyond the scope of this paper and it hasn't been considered in the DOC performance analysis. The evolution of the efficiencies shows very different profiles. On one hand the HC conversion efficiency performs in a quasi-steady behavior along the WLTC cycle. On the opposite, the CO conversion efficiency shows an unstable pattern along most part of the WLTC. This unsteady operation is because of the dependence of the conversion efficiency with the CO inlet concentration and therefore the CO conversion is strongly affected by the transient load conditions. In Fig. 8 the variables that play a main role in the conversion efficiency are shown: CO, HC, oxygen concentration and dwell time. CO concentration performs in a transient manner along the WLTC cycle. Lower CO peaks are observed at -7 ºC than 20 ºC because of the higher air to fuel ratio at low temperatures. HC concentration is greater at -7 ºC during the first 1200 seconds of the WLTC. The HC concentration at -7 ºC becomes lower as the warming up proceeds until it reaches the hydrocarbons level at 20 ºC. The differences observed in O_2 and in dwell time are because of the exhaust mass flow. During the first 600 seconds, exhaust mass flow is higher at -7 ºC

causing lower dwell time and higher oxygen content because of the higher air to fuel ratio. From 600 seconds until the end of the WLTC, both ambient temperature cases show similar dwell times but different oxygen concentrations. The reason of this fact is because of the LP EGR enabling at 20 ºC causing the reduction of both the dwell time, because the higher exhaust mass flow, and the oxygen content, because of the reduction of air to fuel ratio.

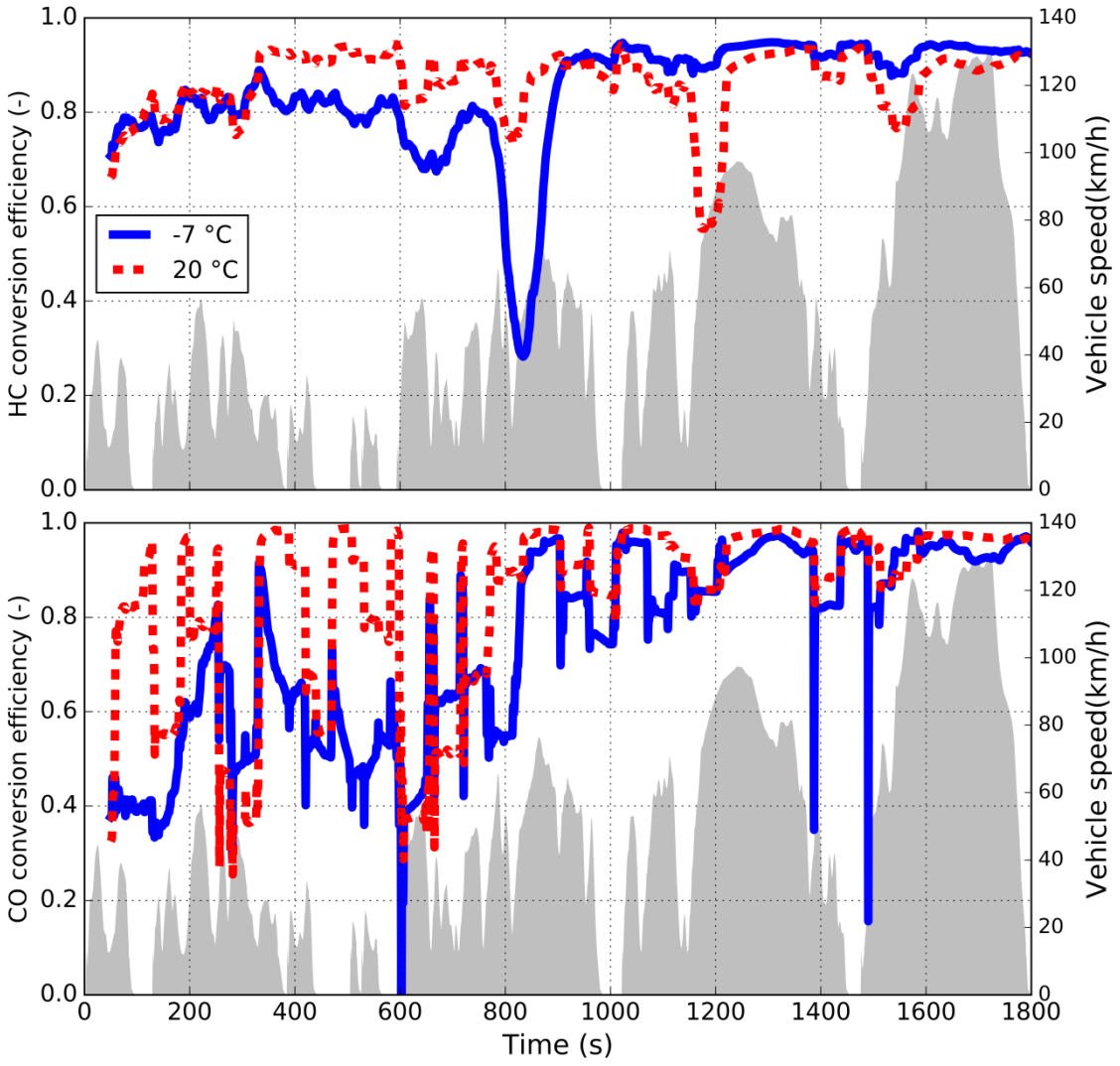

Fig. 7. DOC conversion efficiency for HC and CO. WLTC vehicle speed is depicted as a surface in gray.

The conversion efficiency evolution over the WLTC in Fig. 7 can be deeply analyzed by means of the explanatory variables of Fig. 8. The HC conversion efficiency shows quite high and very similar values from the beginning of the cycle for both ambient temperatures. Between 300 and 800 seconds the efficiency is higher in the case of 20 ºC because of the higher dwell time and lower HC concentration. Despite the lower oxygen concentration at 20 ºC compared to -7ºC, it is still high enough to avoid negative effects on HC conversion. An instant to highlight in the WLTC occurs at 800 seconds, when a notable reduction is detected on HC conversion efficiency in -

7ºC case. The reason of the efficiency reduction in this point is a combination of low dwell time, reduction of oxygen concentration and a sudden increase of CO emissions. The effect of CO concentration peaks on HC conversion is observed many times along the WLTC: 300, 600, 800, 1200 and 1550 seconds are points of HC conversion efficiency reduction because of the interference of CO concentration peaks. In case of 20 ºC two significant efficiency reductions are observed at 1200 and 1550 seconds mainly because of the very low oxygen concentration at these points, which is around 6%. From 1000 seconds, when high and extra-high load are performed, until the end of the WLTC, the HC conversion efficiency is slightly higher in the case of -7ºC than 20 ºC. In the case of -7 ºC, the generation of HC falls to the hydrocarbon concentrations produced at 20ºC and the oxygen concentration keeps higher than 20 ºC. These factors drive to higher conversion efficiency in the case of -7 ºC. Compared to the beginning, at these higher loads of the WLTC parts, the HC conversion shows a steadier profile over time in the case of -7 ºC because of both, the drop of HC formation and the high DOC temperature. As plotted in Fig. 6, the temperature has overcome the 250 ºC threshold, which is considered by many authors as the light-off up limit and beyond that value the conversion efficiency remains constant at the highest value [11, 34]. Regarding CO conversion, the higher the CO peak is, the stronger the CO conversion efficiency drop is. This conversion dependence on CO peaks reduces as the WLTC proceeds. One point to highlight is at 600 seconds where CO DOC efficiency conversion drops because of the change between the HP to the LP EGR system along with the presence of a CO emission peak. The LP EGR enabling increases the exhaust mass flow and therefore the dwell time reduces, driving to lower DOC efficiencies. In the case of THC, as this change is not accompanied with a hydrocarbon emission peak the negative effect in the THC DOC efficiency is less noticeable. Once the WLTC reaches the 800 seconds the drops of CO conversion efficiencies become less important because of the high DOC temperature (250 ºC) and low CO pollutant formation due to engine warming-up. As higher engine loads are performed, the CO conversion efficiency differences between -7 ºC and 20 ºC vanish.

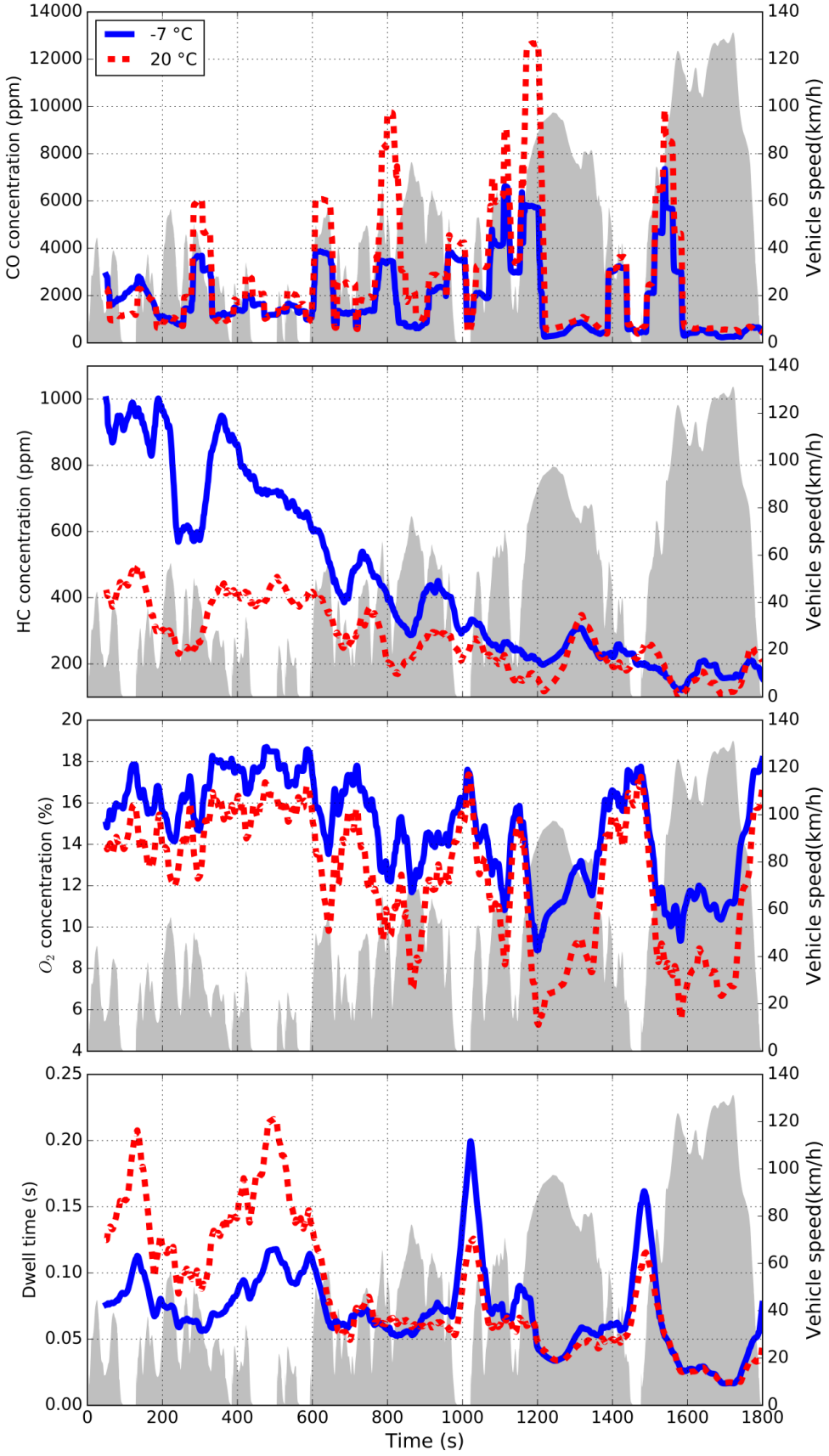

Fig. 8. DOC performance explanatory variables. WLTC vehicle speed is depicted as a surface in gray

4. Conclusions

The effect of low ambient temperatures on pollutant emissions formation and on DOC performance are analysed in this paper. Experimental tests were carried out at transient engine load conditions of WLTC. The pollutants analysis are foccused on carbon monoxide and hydrocarbon emissions.

Regarding the engine-out emissions, the formation of pollutants performs with different behaviours. On the one hand, urburned hydrocarbons show an important dependence on the ambient temperature. At -7 ºC the whole WLTC HC emissions are 2.5 greater than the emissions at 20ºC. On the other hand, carbon monoxide shows a lower dependence with ambient temperature. CO release is strongly affected by transient engine loads because CO formation is driven mainly by the air-fuel mixture conditions. At high and transient loads the air to fuel ratio becomes lower and the incomplete oxidation of CO rises. Owing to this high dependence on air-fuel ratio, the CO production is lower at -7 ºC than at 20 ºC because of the higher air to fuel ratio at lower ambient temperatures.

Concerning the DOC performance, the conversion efficiency of CO and HC shows very different evolutions. Hydrocarbons conversion performs in a steadier way along the WLTC than the carbon monoxide, which is deeply affected by the CO peaks generation at the transient engine load conditions. For most of the WLTC low and medium load cycle part, the conversion efficiency for both pollutants is higher at 20 ºC than at -7 ºC. As the engine load increases (high and extra high WLTC parts) conversion efficiency differences vanish and even the HC conversion shows slighlty higher efficiencies at -7ºC than at 20ºC. While HC conversion shows relative low differences between both ambient temperatures, in the case of CO the DOC performance is considerably worse at -7ºC than at 20ºC.

Aknowledgments

The authors of this paper wish to thank Juan Antonio López Cascant for his invaluable work during the laboratory setup and the experimental campaign. Authors also want to acknowledge the “Apoyo para la investigación y Desarrollo (PAID)”, grant for doctoral studies (FPI S1 2015 2512), of Universitat Politècnica de València.

References

1. Reşitoğlu, İ.A., Altinişik, K. & Keskin, A. The pollutant emissions from diesel-engine vehicles and exhaust aftertreatment systems, Clean Techn Environ Policy (2015) 17: 15.

2. Johnson, T. (2014). Vehicular emissions in review. SAE International Journal of Engines, 7(2014-01-1491), 1207-1227.

3. Qinming Tan, Yihuai Hu, A study on the combustion and emission performance of diesel engines under different proportions of O2 & N2 & CO2, Applied Thermal Engineering, Volume 108, 5 September 2016, Pages 508-515.

4. Wenyi Liu, Chonglin Song, Effect of post injection strategy on regulated exhaust emissions and particulate matter in a HSDI diesel engine, Fuel, Volume 185, 1 December 2016, Pages 1-9

5. Justin D.K. Bishop, Marc E.J. Stettler, N. Molden, Adam M. Boies, Engine maps of fuel use and emissions from transient driving cycles, Applied Energy, Volume 183, 1 December 2016, Pages 202-217.

6. Kevin Koosup Yum, Nicolas Lefebvre, Eilif Pedersen, An experimental investigation of the effects of cyclic transient loads on a turbocharged diesel engine, Applied Energy, Volume 185, Part 1, 1 January 2017, Pages 472-481.

7. Serrano, J. R., Arnau, F. J., Martin, J., Hernandez, M., & Lombard, B. (2015). Analysis of Engine Walls Thermal Insulation: Performance and Emissions (No. 2015-01-1660). SAE Technical Paper.

8. H. Santos, M. Costa, Evaluation of the conversion efficiency of ceramic and metallic three way catalytic converters, Energy Conversion and Management, Volume 49, Issue 2, February 2008, Pages 291-300.

9. J.M. Herreros, S.S. Gill, I. Lefort, A. Tsolakis, P. Millington, E. Moss, Enhancing the low temperature oxidation performance over a Pt and a Pt–Pd diesel oxidation catalyst, Applied Catalysis B: Environmental, Volume 147, 5 April 2014, Pages 835-841.

10. S. Salomons, M. Votsmeier, R.E. Hayes, A. Drochner, H. Vogel, J. Gieshof (2006). CO and H2 oxidation on a platinum monolith diesel oxidation catalyst, Catalysis Today, Volume 117, Issue 4, Pages 491-497.

11. Zervas, E. (2008).Parametric study of the main parameters influencing the catalytic efficiency of a diesel oxidation catalyst: Parameters influencing the efficiency of a diesel catalyst. Int.J Automot. Technol. 9: 641

12. Botsaris, P. N., & Sparis, P. D. (2000). Ambient temperature influence on catalytic outlet—inlet temperature difference. Proceedings of the Institution of Mechanical Engineers, Part D: Journal of Automobile Engineering, 214(1), 95-100.

13. Karl Arnby, Anders Törncrona, Bengt Andersson, Magnus Skoglundh, Investigation of Pt/γ-Al2O3 catalysts with locally high Pt concentrations for oxidation of CO at low temperatures, Journal of Catalysis, Volume 221, Issue 1, 1 January 2004, Pages 252-261.

14. Torregrosa, A. J., Olmeda, P., Martin, J., & Degraeuwe, B. (2006). Experiments on the influence of inlet charge and coolant temperature on performance and emissions of a DI Diesel engine. Experimental Thermal and Fluid Science, 30(7), 633-641.

15. Torregrosa, A. J., Broatch, A., Olmeda, P., & Romero, C. (2008). Assessment of the influence of different cooling system configurations on engine warm-up, emissions and fuel consumption. International Journal of Automotive Technology, 9(4), 447-458.

16. Weilenmann, M., Favez, J. Y., & Alvarez, R. (2009). Cold-start emissions of modern passenger cars at different low ambient temperatures and their evolution over vehicle legislation categories. Atmospheric environment, 43(15), 2419-2429.

17. Ludykar, D., Westerholm, R., & Almen, J. (1999). Cold start emissions at+ 22,− 7 and− 20 C ambient temperatures from a three-way catalyst (TWC) car: regulated and unregulated exhaust components. Science of the Total Environment, 235(1), 65-69.

18. Weilenmann, M., Soltic, P., Saxer, C., Forss, A. M., & Heeb, N. (2005). Regulated and nonregulated diesel and gasoline cold start emissions at different temperatures. Atmospheric environment, 39(13), 2433-244.

19. Gumus, M. (2009). Reducing cold-start emission from internal combustion engines by means of thermal energy storage system. *Applied thermal engineering*, *29*(4), 652-660.

20. Luján, J. M., Climent, H., Dolz, V., Moratal, A., Borges-Alejo, J., & Soukeur, Z. (2016). Potential of exhaust heat recovery for intake charge heating in a diesel engine transient operation at cold conditions. Applied Thermal Engineering, 105, 501-508.

21. Robinson, K., Ye, S., Yap, Y., & Kolaczkowski, S. T. (2013). Application of a methodology to assess the performance of a full-scale diesel oxidation catalyst during cold and hot start NEDC drive cycles. Chemical Engineering Research and Design, 91(7), 1292-1306.

22. Messer, J. T., Clark, N. N., & Lyons, D. W. (1995). Measurement delays and modal analysis for a heavy duty transportable emissions testing laboratory (No. 950218). SAE Technical Paper.

23. Konstantas, G., & Stamatelos, A. (2004). Quality assurance of exhaust emissions test data. Proceedings of the Institution of Mechanical Engineers, Part D: Journal of Automobile Engineering, 218(8), 901-914.

24. Pakko, J. D. (2009). Reconstruction of Time-Resolved Vehicle Emissions Measurements by Deconvolution. SAE International Journal of Fuels and Lubricants, 2(2009-01-1513), 697-707.

25. Directive 97/68/EC of the European Parliament and of the Council of 16 December 1997 on the approximation of the laws of the Member States relating to measures against the emission of gaseous and particulate pollutants from internal combustion engines to be installed in non-road mobile machinery. http://eur-lex.europa.eu/legal-content/EN/TXT/?uri=CELEX:31997L0068

26. Kandylas, I. P., Stamatelos, A. M., & Dimitriadis, S. G. (1999). Statistical uncertainty in automotive emissions testing. Proceedings of the Institution of Mechanical Engineers, Part D: Journal of Automobile Engineering, 213(5), 491-502.

27. Morgan, V. T. (1975). The overall convective heat transfer from smooth circular cylinders. Advances in heat transfer, 11, 199-264.

28. Koop, J., & Deutschmann, O. (2009). Detailed surface reaction mechanism for Pt-catalyzed abatement of automotive exhaust gases. Applied Catalysis B: Environmental, 91(1), 47-58.

29. Payri, F., Bermúdez, V. R., Tormos, B., & Linares, W. G. (2009). Hydrocarbon emissions speciation in diesel and biodiesel exhausts. Atmospheric Environment, 43(6), 1273-1279.

30. Bohac, S. V., Han, M., Jacobs, T. J., López, A. J., Assanis, D. N., & Szymkowicz, P. G. (2006). Speciated hydrocarbon emissions from an automotive diesel engine and DOC utilizing conventional and PCI combustion (No. 2006-01-0201). SAE Technical Paper.

31. Burke, R. D., Brace, C. J., Lewis, A., Cox, A., & Pegg, I. (2011). Analysis of energy flows in engine coolant, structure and lubricant during warm-up. In Vehicle Thermal Management Systems Conference and Exhibition, VTMS 10 (pp. 167-176). University of Bath.

32. Lefort, I., Herreros, J. M., & Tsolakis, A. (2014). Reduction of low temperature engine pollutants by understanding the exhaust species interactions in a diesel oxidation catalyst. Environmental science & technology, 48(4), 2361-2367.

33. Patterson, M. J., Angove, D. E., & Cant, N. W. (2000). The effect of carbon monoxide on the oxidation of four C 6 to C 8 hydrocarbons over platinum, palladium and rhodium. Applied Catalysis B: Environmental, 26(1), 47-57.

34. Johnson, T. V. (2010). Review of diesel emissions and control. SAE International Journal of Fuels and Lubricants, 3(2010-01-0301), 16-29.

35. Kamijo, M., Kamikubo, M., Akama, H., & Matsushita, K. (2001). Study of an oxidation catalyst system for diesel emission control utilizing HC adsorption. JSAE review, 22(3), 277-280.

36. Hiramoto, Y., Takaya, M., Yamamoto, S., & Okada, A. (2003). Development of a new HC-adsorption three-way catalyst system for partial-ZEV performance (No. 2003-01-1861). SAE Technical Paper.